ACS SENSORS
Article
pubs.acs.org/acssensors

Large-Area Low-Cost Plasmonic Perfect Absorber Chemical Sensor Fabricated by Laser Interference Lithography

Shahin Bagheri,[†] Nikolai Strohfeldt,[†] Florian Sterl,[†] Audrey Berrier,[‡] Andreas Tittl,[†,§] and Harald Giessen*,[†]

[†]4th Physics Institute and Research Center SCoPE and [‡]1st Physics Institute and Research Center SCoPE, University of Stuttgart, 70569 Stuttgart, Germany

[§]Institute of BioEngineering, École Polytechnique Fédérale de Lausanne (EPFL), CH-1015 Lausanne, Switzerland

S *Supporting Information*

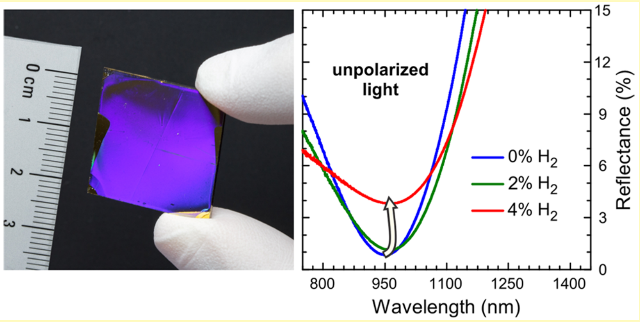

ABSTRACT: We employ laser interference lithography as a reliable and low-cost fabrication method to create nanowire and nanosquare arrays in photopolymers for manufacturing plasmonic perfect absorber sensors over homogeneous areas as large as 5.7 cm^2. Subsequently, we transfer the fabricated patterns into a palladium layer by using argon ion beam etching. Geometry and periodicity of our large-area metallic nanostructures are precisely controlled by adjusting the interference conditions during single- and double-exposure processes, resulting in active nanostructures over large areas with spectrally selective perfect absorption of light from the visible to the near-infrared wavelength range. In addition, we demonstrate the method's applicability for hydrogen detection schemes by measuring the hydrogen sensing performance of our polarization independent palladium-based perfect absorbers. Since palladium changes its optical and structural properties reversibly upon hydrogenation, exposure of the sample to hydrogen causes distinct and reversible changes within seconds in the absorption of light, which are easily measured by standard microscopic tools. The fabricated large-area perfect absorber sensors provide nearly perfect absorption of light at 730 and 950 nm, respectively, and absolute reflectance changes from below 1% to above 4% in the presence of hydrogen. This translates to a relative signal change of almost 400%. The large-area and fast manufacturing process makes our approach highly attractive for simple and low-cost sensor fabrication, and therefore, suitable for industrial production of plasmonic devices in the near future.

KEYWORDS: *plasmonics, perfect absorber, hydrogen sensing, large-area fabrication, laser interference lithography*

The interaction of light with metallic nanostructures reveals unique optical properties originating from the excitation of localized surface plasmon resonances.[1−4] Among the intriguing optical effects found in such systems, high or perfect absorption of light at a specific wavelength is used for a wide range of applications such as photovoltaic efficiency enhancement,[5,6] color printing,[7,8] spectroscopy,[9,10] and sensing.[11,12] Tuning of the perfect absorption wavelength, which is highly desirable especially for sensing applications, can be realized by adjusting the size and shape of the constituent nanostructures.[13,14] Perfect-absorber-based plasmonic sensors have attracted significant interest in recent years, owing to their ability to detect minute changes in the optical properties of the involved materials. This is highly important in the context of hydrogen (H_2) sensing, where small amounts of hydrogen gas in the air can already lead to highly dangerous and explosive gas mixtures.[15] There are several materials that change their optical or mechanical properties upon hydrogen exposure and can, therefore, be used in optical sensing schemes, such as palladium,[16] yttrium,[17] and magnesium.[18] Other than palladium, where the change of the dielectric properties due to hydrogenation leads to a shift of the plasmonic resonance, yttrium and magnesium undergo a complete phase transition from a metallic into a dielectric state. However, their lack of catalytic properties requires the addition of catalytic palladium or platinum elements to facilitate hydrogen dissociation, increasing the complexity of the nanostructures.

The concept of plasmonic perfect absorption is based on the efficient coupling of incident light into the structure through matching of its optical impedance to the impedance of the surrounding medium, leading to a near-complete suppression of reflection (R) for a certain design wavelength.[19] By simultaneously suppressing the transmission (T) through the structure, near-perfect absorption can be obtained. In the visible wavelength range, this can be achieved by utilizing a perfect absorber consisting of palladium nanowires, separated from a gold covered substrate by a magnesium fluoride spacer layer.[20]

Received: July 18, 2016
Accepted: August 24, 2016
Published: August 24, 2016

DOI: 10.1021/acssensors.6b00444
ACS Sens. 2016, 1, 1148−1154

As mentioned already, the reflection can then be tuned to nearly zero by carefully adjusting the geometrical parameters of the system to provide perfect impedance matching of the vacuum impedance and consequently maximizing the absorbance $A = 1 - T - R$ to almost 1. This measurement scheme is highly interesting for many sensing applications since it provides a high contrast ratio, going from (almost) no signal to a significantly higher signal at the position of minimum reflectance. Even if imperfect absorption (for example, a value over 90% but not over 99%) is achieved, the enhanced relative signal change is advantageous for any kind of sensor.

Precisely defined and tailored nanostructures are essential for realizing such nanoplasmonic sensor schemes. Electron-beam lithography is a commonly used method to create well-defined masks for the fabrication of plasmonic perfect absorbers over small areas. However, a fabrication method for producing perfect absorbers in a low-cost and high-throughput manner over large areas is crucial to advance plasmonic sensors toward technological applications. Other methods such as self-assembly,[21] chemical synthesis,[22] metal nanoparticle deposition,[23,24] colloidal etching lithography,[25] and nanoimprint lithography[26,27] have been proposed for the fabrication of plasmonic structures over large areas, but often suffer from large-scale inhomogeneity. Compared to other promising large-area fabrication methods, laser interference lithography (LIL)[28] shares many of the advantages of other lithographic techniques while alleviating a majority of concerns such as cost and complexity. It also provides well-defined, defect-free, and homogeneous arrays of nanostructures over large areas, enabling high-performance perfect absorbers on the wafer scale. Through wafer-scale production, standardized and robust measurement schemes with macroscopic cm^2-sized samples are possible, providing carefree user-friendly devices.

In this work, we employ laser interference lithography and subsequent argon ion beam etching to fabricate large-area plasmonic perfect absorbers. We first fabricate a perfect absorber sensor geometry based on palladium nanowire arrays and demonstrate its hydrogen sensing performance. This geometry provides highly sensitive hydrogen detection but requires the incident light to be polarized perpendicular to the wires. Therefore, we subsequently extend this concept toward the fabrication of large-area palladium based perfect absorber sensors with rectangular nanoantennas, which provide perfect absorption of light independent of the incident polarization. Extensive numerical simulations are carried out to find an optimal design, and the hydrogen sensing performance of a fabricated polarization-independent sensor is investigated. Our high-throughput and low-cost fabrication method combined with the simple concept of a plasmonic device that provides pronounced signal changes in response to external stimuli makes our sensor well suited for real-world applications.

EXPERIMENTAL SECTION

Sample Fabrication. In preparation for the fabrication process, fused silica substrates are cleaned with acetone and isopropanol for 10 min in an ultrasonic bath. After that, 2 nm of chromium (Cr, adhesion layer) followed by 150 nm gold (Au, mirror), magnesium fluoride (MgF_2, spacer), and palladium (Pd, hydrogen sensitive material) are evaporated onto the substrate (Pfeiffer vacuum model PLS-500, 10^{-7} mbar). Afterward, a 90-nm-thick photoresist film (ma-N 405) is spin-coated on top of the Pd layer. For the subsequent exposure process, we use an expanded light beam of a He−Cd laser ($\lambda = 325$ nm) and a Lloyd's mirror setup.[29] Typical UV exposure doses are about 1 mJ/cm^2 with typical exposure times of 30 s. To achieve two-dimensional structures, the sample is rotated 90° followed by a second exposure process. Subsequently, the sample is immersed into the development solution (AZ 826) for 30 s. The areas covered with the developed photoresist are then transferred into the Pd layer via an argon ion beam etching process (Technics Plasma model R.I.B.-Etch 160, beam current range from 90 to 100 mA, typical etching times between 70 and 100 s). Finally, the remaining photoresist is removed using isopropanol followed by O_2 plasma treatment (Diener Electronic Plasma-Surface-Technology, 90 min, 1.4 mbar, 160 W).

Reflection Measurements. The angle-resolved reflectance measurements are performed via a free-space, goniometer-based angular-resolved reflectivity setup. The light intensity from a xenon lamp, coupled to a monochromator and polarized using input polarizer, is detected via a silicon detector with output analyzer. The light beam is highly collimated (angular divergence smaller than 0.15°) and has a diameter of about 1 mm. The incident angle was varied between 20° and 50° in steps of 10°. The reflectance level of a Herasil sample, compared to its ideal value, is used as a reference to compensate for small setup deviations.

The gas concentration-dependent and independent reflection measurements under normal incidence are performed using a commercial Fourier transform infrared spectroscopy system (Bruker FTIR), allowing for laterally resolved measurements on the micrometer scale. For the hydrogen-dependent measurements, the sample is mounted in a custom-made vacuum-tight gas cell connected to Bronkhorst mass flow controllers that regulate and monitor the hydrogen and nitrogen gas flows during the measurement with very high accuracy (0.5% Rd).

Photograph and Scanning Electron Micrographs. The photograph was taken with a Canon EOS 60D camera with a Canon EF 100 mm f/2.8 Macro USM (f/8, 1/4 s, ISO 100). The sample was illuminated with a large diffuse light source (daylight color temperature). The scanning electron micrographs were acquired with an S-4800 scanning electron microscope (Hitachi Company).

RESULTS AND DISCUSSION

Laser interference lithography is a low-cost fabrication method to prepare homogeneous nanostructures over large areas. It relies on the interference of two coherent laser beams, which produces a standing wave grating pattern that can be transferred to a light sensitive photoresist for the preparation of one-dimensional wire structures.[30] Furthermore, the addition of a second exposure process enables the fabrication of geometrically tunable 2D-nanostructures.[28,31] Such nanostructures are transferable to metal via a subsequent etching process.[28,32,33] Here, we utilize single- and double-exposure processes to fabricate homogeneous palladium nanowire and rectangle arrays for plasmonic perfect absorbers.

A photograph and a scanning electron microscope (SEM) image of a typical perfect absorber fabricated using laser interference lithography (sample size of 2.4 × 2.4 cm^2) are shown in Figure 1a and b, respectively, demonstrating the large-area nature and homogeneity of the sample. The periodicity of the depicted grating is 450 nm, the wire width is 120 nm, the spacer height is 65 nm, and the Pd structures have a thickness of 20 nm. The homogeneity is additionally confirmed by reflectivity measurements of five different areas of the sample (indicated as colored points in the inset of Figure 1c). The measurements show less than 5% deviation in spectral location and modulation depth (Figure 1c) and a typical reflectance measurement for polarization perpendicular to the wires shows a minimum reflectance of about 1% (in the optimal case) and thus nearly perfect absorption of light at the resonance wavelength of $\lambda = 740$ nm (blue curve).

The optical properties of the Pd nanowires are modified in the presence of H_2 through the phase transition from palladium

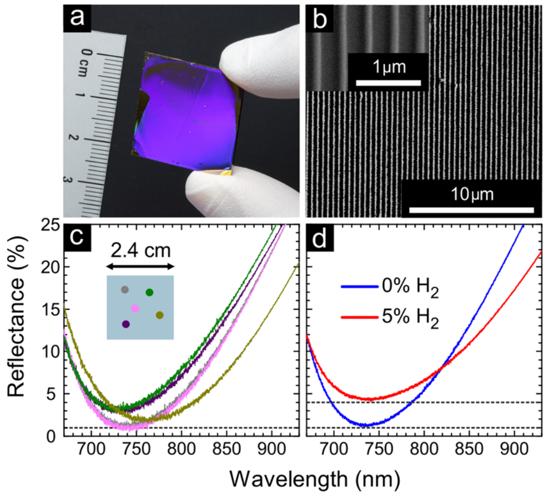

Figure 1. Large-area palladium-based one-dimensional perfect absorber sensor fabricated by laser interference lithography. (a) Photograph and (b) scanning electron microscope (SEM) image of a typical sample showing the homogeneity of the plasmonic structures over large areas. (c) Homogeneity is also confirmed by reflection measurements of five different areas of the sample. (d) Reflectivity of the sample (blue line, about 1% minimum reflectance) undergoes a pronounced increase after exposure to 5 vol % hydrogen in nitrogen carrier gas (red line, about 4% minimum reflectance). The typical sample size is 2.4 × 2.4 cm^2.

to palladium hydride (PdH).[34] The significant change in the real and imaginary parts of the palladium dielectric function destroys the optimized impedance matching condition of the perfect absorber and consequently changes the reflectivity profile of the system. This can be observed in the spectra as a spectral red-shift of about 10 nm and an increase of the minimum reflectance from 1% to 4% when exposing the sample to 5.0 vol % hydrogen in nitrogen (N_2) carrier gas (Figure 1d).

However, to bring this approach to technological and life-science applications, a polarization independent system with two-dimensional symmetric nanostructures is required. This is easily achievable using laser interference lithography in a double-exposure process. The schematic side view of such a perfect absorber is depicted in Figure 2a, where square palladium nanoantennas are stacked above a gold mirror separated by a MgF_2 spacer layer. To estimate the optical properties of our structure, we perform simulations using a scattering matrix method[35] to calculate the reflectance spectra of square nanoantenna arrays (periodicity 560 nm, Pd thickness 30 nm) for different square widths and spacer heights. Afterward, we extract the lowest reflectance (Figure 2b) and the corresponding spectral location of the minimum (Figure 2c). The figures indicate that square widths between 160 and 250 nm and spacer heights between 70 and 75 nm are expected to provide the best results. A target point with the square width of about 190 nm and spacer height of about 71 nm is indicated by the white circle and dashed lines in the color plots. The reflectance is shown in a logarithmic color scale for better visibility.

According to the simulations, the working range of our large-area perfect absorber can be tuned from 800 to 1300 nm by changing the rectangle size from 150 to 250 nm. The main experimental constraint for tunability is given by the fact that the laser interference method only allows nanostructure sizes between 20% and 75% of the periodicity (560 nm in our case).

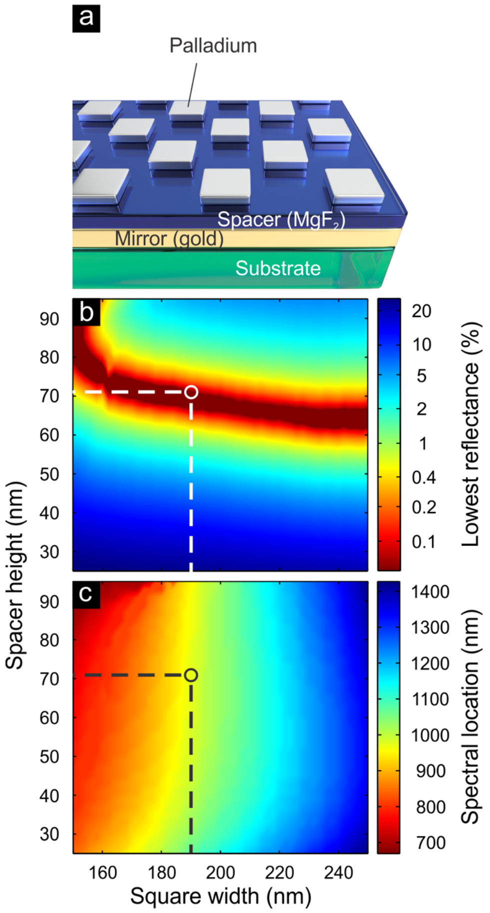

Figure 2. (a) Schematic view of the large-area perfect absorber sensor. (b) Simulated minimum reflectance for different square widths and spacer heights. The suitable parameters for a perfect absorber are located in the dark red area. The reflectance is shown in a logarithmic color scale for better visibility. (c) Spectral locations of the minimum reflectance (i.e., perfect absorption) for corresponding square widths and spacer heights. The target square width and spacer height for fabrication are indicated by the white circle.

Nevertheless, our Lloyd's mirror setup enables full control of the periodicity from the UV up to about 900 nm and therefore full tunability of the square widths. Even higher periodicities are accessible using other laser interference lithography setups.[28,30]

To achieve polarization-independent perfect absorption of light over large areas, we fabricate palladium square arrays (periodicity 560 nm, square width 190 nm). An SEM image of the sample is shown in Figure 3a, demonstrating high homogeneity over large areas. The angular behavior of the structure is studied by angle-resolved reflectance measurement for both p- and s-polarization (Figure 3b and c, respectively).

In both polarizations, the minimum reflectance remains below 7% for incident angles up to 50°. This means that our device is able to maintain near-perfect absorption even at high angles, making it a good candidate for technological applications. The small observed changes in reflectance at higher angles are expected for arrayed elements due to the onset of evanescent grating modes, and can only be avoided by using plasmonic perfect absorbers with disordered structures.[36]

The reflectance spectrum of the fabricated perfect absorber at normal incidence and excitation by unpolarized light shows nearly perfect absorption (i.e., $R = 1\%$) at the target wavelength of 950 nm (Figure 4a, blue line). This is in excellent agreement

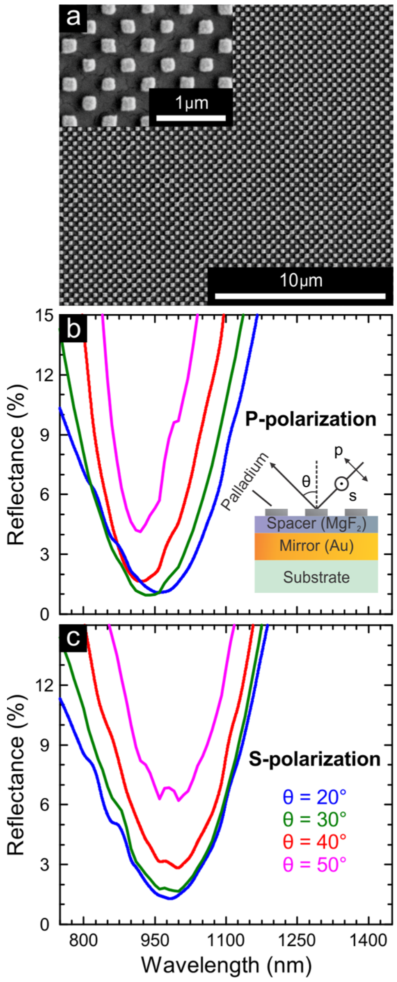

Figure 3. (a) SEM image of square palladium nanoantenna arrays utilized in a large-area plasmonic perfect absorber sensor fabricated by laser interference lithography. (b,c) Angle-resolved reflection measurements for p- and s-polarization show a residual reflectance below 7% for incident angles up to 50°. In p-polarization, the reflectance spectra shift to lower wavelengths for higher incident angles, whereas the spectral location of lowest reflectance in s-polarization remains constant.

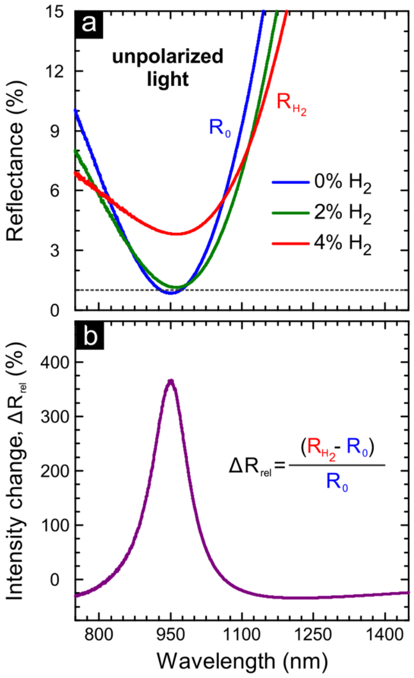

Figure 4. (a) Reflection measurement of the large-area perfect absorber for different H_2 concentrations in the N_2 carrier gas. The initial reflectance of the sample (blue line) increases after hydrogen exposure (green line, 2%; red line, 4% hydrogen in nitrogen). (b) Relative reflectance change (ΔR_{rel}) between 0% and 4% hydrogen concentrations over wavelength, indicating signal changes of almost 400%.

with our simulations (see Figure 2b,c). Small differences are expected since the nanostructuring process, including evaporation, photoresist patterning, and etching, can introduce impurities and defects into the system.

Exposing the sample to low hydrogen concentrations (e.g., 2 vol % H_2 in N_2 or less) causes only small changes in the minimum reflectance of the perfect absorber. However, a distinct wavelength shift to higher wavelengths (about 9 nm) and a slight decrease of the absorbance (Figure 4a, green line) can be seen. Using higher hydrogen partial pressures (4 vol % H_2 in N_2 and more) causes a pronounced change of the reflectance spectrum. In addition to a wavelength red-shift of about 13 nm, a dramatic spectral broadening of the reflection profile as well as a reflectivity increase from 1% to about 5% (Figure 4a, red line) is visible. The strong relative intensity changes of about 400% at the minimum reflectance wavelength, induced by relatively small changes in environmental hydrogen concentration, demonstrate the performance advantages of the perfect absorber sensing scheme (Figure 4b). Since the palladium/hydrogen interaction is reversible, the minimum reflectance of the system returns to its initial state of almost perfect absorption after removing H_2 from the atmosphere.

To investigate this sensitivity of our perfect absorber to hydrogen gas in detail, we fabricated a second sample with the reflectance minimum at about 900 nm. We expose it to various hydrogen concentrations and continuously monitor changes in reflectance over time, during both the loading and unloading processes (Figure 5a). After a pure N_2 atmosphere, the concentration sequence starts with 600 s of 0.5 vol % H_2 in N_2, followed by 2000 s of pure nitrogen, then 600 s at 1 vol % H_2 and so on, until a maximum H_2 concentration of 10 vol % is reached.

The temporal and spectral response of the perfect absorber sensor during hydrogen exposure is shown as a color-coded plot in Figure 5a, indicating the wavelength shift as well as the reflectance (R) change for each spectrum on a logarithmic color scale. To quantify the spectral shift of the perfect absorber resonance during the concentration sequence, the centroid wavelength (CWL) is calculated from the FTIR reflectance measurements, which enables the detection of small resonance shifts independent of the shape and noise characteristics of the spectral features.[37] The initial reflectance minimum (at 897 nm) undergoes a 3 nm shift to higher wavelengths when applying a hydrogen concentration of 0.5 vol % H_2 in N_2 and further red-shifts when higher hydrogen concentrations are applied (see Figure S1 and the video file in Supporting Information).

The time traces of the reflection at different wavelengths are shown in the Supporting Information (Figure S2) which indicates that the changes in reflection become smoother with increasing wavelength. In Figure 5b, the time trace of the reflection at 1150 nm for H_2 concentrations up to 10% is

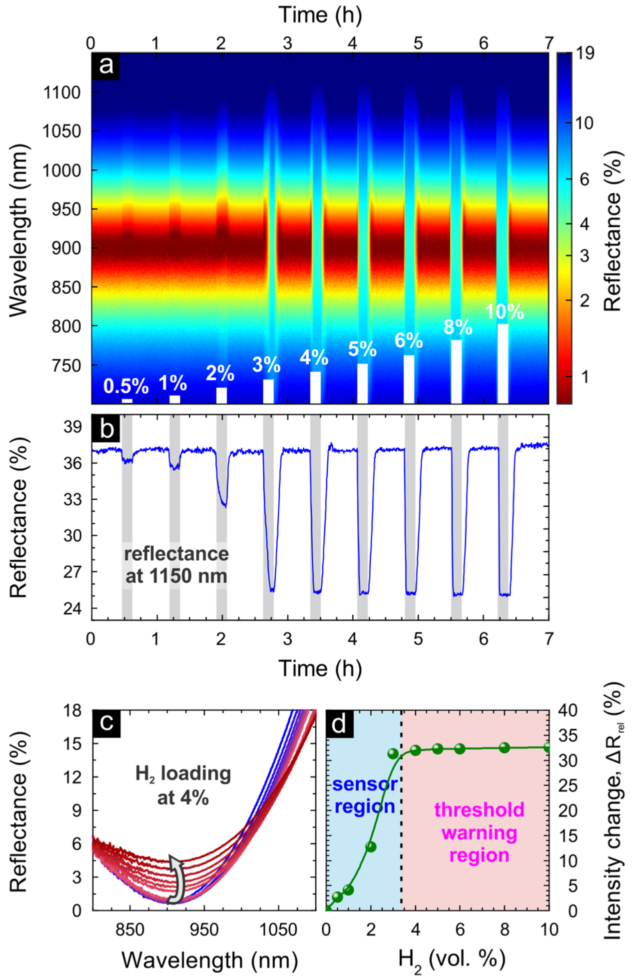

Figure 5. Time-resolved spectral response of the palladium based plasmonic perfect absorber sensor during exposure to hydrogen gas. (a) Color-coded plot of time-dependent reflectance spectra for different hydrogen concentrations (white colored bars). The sample is exposed to different hydrogen concentrations for 600 s and to pure nitrogen for 2000 s after each hydrogen step. The time-step for the recorded spectra is 15 s. (b) Time trace of the reflection of the large-area perfect absorber sensor at 1150 nm for different hydrogen concentrations. (c) Evolution of the reflectance spectra of the plasmonic perfect absorber during 4 vol % H_2 loading. The minimum reflectance initially red-shifts (Pd in α-phase) and then shifts into the blue with strongly increasing reflectance and broadening of the spectra, when Pd transforms into the β-phase. (d) Relative intensity change of the perfect absorber at different hydrogen concentrations splitting the functionality of the sample into a quantitative sensor region (blue area, Pd in α-phase) and a threshold warning region for hydrogen concentrations of 3% or more (red area, Pd in β-phase).

depicted. The initial reflectance (at 37%) undergoes a 1% decrease when applying a hydrogen concentration of 0.5 vol % H_2 in N_2 and is further reduced when higher hydrogen concentrations are applied. When exposing the sensor to 2 vol % of H_2, a pronounced and slow change of the reflectance is observed, which can be understood by considering the hydrogen-induced phase-transition in palladium. In the case of palladium nanoparticles, this transition between α- and β-phase starts to occur at hydrogen partial pressures of about 20 mbar (2 vol % H_2 at atmospheric pressure) at room temperature.[34,38] Through exposure to higher hydrogen partial pressures, the palladium patches are fully transformed into the β-phase, resulting in a quasi-saturation of the sensor.[39,40] The same measurement is carried out for the sample in Figure 4, showing a similar behavior (Figure S3 in the Supporting Information). The stability of the sensor device over multiple gas exposure cycles is confirmed by carrying out a second measurement on the same sample (see also Figure S3 in the Supporting Information).

Full reflectance spectra illustrating the evolution of the optical response during this hydrogen loading cycle are displayed in Figure 5c. When the H_2 loading starts, the Pd is first transformed into PdH_x in the α-phase with $x > 0.2$. This phase has different optical properties than pure Pd but almost no effect on the lattice spacing between the palladium atoms,[41] resulting in a small modification of the perfect absorber's optical response (red-shift of the minimum reflectance). Exposure to higher H_2 partial pressures leads to a phase change into the PdH_x β-phase ($x \cong 0.7$), which is accompanied by a drastic change in nanoantenna volume of up to 12%[42] in addition to a change in the electronic and, therefore, dielectric properties. The expansion seems to be dominated by a growth in the direction perpendicular to the surface due the excellent adhesion of Pd to the MgF_2 spacer layer. This thickness increase of the nanoantennas leads to an overall blue-shift of the resonance.[38]

Figure 5d shows the equilibrium intensity changes of our perfect absorber device at 1150 nm for different H_2 concentrations. The minimum reflectance was extracted at each H_2 concentration step right before the subsequent unloading process. At H_2 concentrations below 3.5 vol %, we observe a near-linear relation between the relative intensity changes and the applied hydrogen concentration. Therefore, in this concentration range, the system can be operated as a quantitative sensor for hydrogen in the environment (blue area). At higher concentrations, the amplitude stays mostly constant and the system can still be utilized as a threshold warning device (red area).

The fabricated plasmonic perfect absorber sensor can be optimized for special applications where the fast response or maximum wavelength shift to H_2 exposure is required by using other novel material such as yttrium,[17] magnesium,[18] and titanium dioxide[43] or by using direct contact palladium–gold nanostructures.[44,45]

■ CONCLUSION

In summary, we have utilized laser interference lithography to fabricate large-area palladium wire and square nanoantenna arrays with excellent homogeneity, to realize plasmonic perfect absorber sensors in the visible and near-infrared spectral wavelength ranges. The fabricated perfect absorbers provide near-zero reflection at specific design wavelengths, which translates to almost 100% absorption of light. The working wavelength of our perfect absorber can be tuned over a wide range, as demonstrated by different fabricated samples as well as extensive scattering matrix simulations. Additionally, we measured the optical response of our large-area sensor in the presence of hydrogen and observed relative intensity changes of up to 400% at hydrogen concentrations of above 3 vol % in N_2. The simplicity and versatility of our large-area and low-cost fabrication process will enable the further development of perfect absorber sensors into a fascinating tool for the optical detection of small amounts of hydrogen or other trace gases in a multitude of industrial applications.

■ ASSOCIATED CONTENT

Ⓢ Supporting Information

The Supporting Information is available free of charge on the ACS Publications website at DOI: 10.1021/acssensors.6b00444.

> Optical response of the palladium based plasmonic perfect absorber sensor; time trace of the reflection of the large-area perfect absorber sensor; time-resolved optical response of the palladium based plasmonic perfect absorber sensor (PDF)
>
> Reflectance time trace (upper panel) as well as centroid wavelength time trace (lower panel) of large-area perfect absorber for different hydrogen concentrations (AVI)

■ AUTHOR INFORMATION

Corresponding Author

*E-mail: h.giessen@pi4.uni-stuttgart.de.

Author Contributions

All authors have given approval to the final version of the manuscript.

Notes

The authors declare no competing financial interest.

■ ACKNOWLEDGMENTS

The authors gratefully acknowledge financial support by ERC Advanced Grant COMPLEXPLAS as well as DFG, BMBF, Zeiss foundation, MWK Baden-Württemberg, and the Baden-Württemberg Stiftung. The authors also thank Dominik Floess for sample photography and Martin Schäferling for the assistance in S-matrix simulation.

■ ABBREVIATIONS

R, reflection; *T*, transmission; *A*, absorbance; LIL, laser interference lithography; CWL, centroid wavelength; ΔR_{rel}, relative reflectance change

■ REFERENCES

(1) Tame, M. S.; McEnery, K. R.; Özdemir, S. K.; Lee, J.; Maier, S. A.; Kim, M. S. Quantum plasmonics. *Nat. Phys.* **2013**, *9*, 329−340.

(2) Berweger, S.; Atkin, J. M.; Olmon, R. L.; Raschke, M. B. Light on the tip of a needle: plasmonic nanofocusing for spectrometry on the nanoscale. *J. Phys. Chem. Lett.* **2012**, *3*, 945−952.

(3) Willets, K. A.; Van Duyne, R. P. Localized surface plasmon resonance spectroscopy and sensing. *Annu. Rev. Phys. Chem.* **2007**, *58*, 267−297.

(4) Mayer, K.; Hafner, J. Localized Surface Plasmon Resonance Sensors. *Chem. Rev.* **2011**, *111*, 3828−3857.

(5) Vora, A.; Gwamuri, J.; Pala, N.; Kulkarni, A.; Pearce, J. M.; Güney, D. Ö. Exchanging ohmic losses in metamaterial absorbers with useful optical absorption for photovoltaics. *Sci. Rep.* **2014**, *4*, 4901.

(6) Pillai, S.; Green, M. Plasmonics for photovoltaic applications. *Sol. Energy Mater. Sol. Cells* **2010**, *94*, 1481−1486.

(7) Roberts, A. S.; Pors, A.; Albrektsen, O.; Bozhevolnyi, S. I. Subwavelength plasmonic color printing protected for ambient use. *Nano Lett.* **2014**, *14*, 783−787.

(8) Cheng, F.; Gao, J.; Luk, T. S.; Yang, X. D. Structural color printing based on plasmonic metasurfaces of perfect light absorption. *Sci. Rep.* **2015**, *5*, 11045.

(9) Chen, K.; Adato, R.; Altug, H. Dual-band perfect absorber for multispectral plasmon-enhanced infrared spectroscopy. *ACS Nano* **2012**, *6*, 7998−8006.

(10) Li, Y.; Su, L.; Shou, C.; Yu, C.; Deng, J.; Fang, Y. Surface-enhanced molecular spectroscopy (SEMS) based on perfect-absorber metamaterials in the mid-infrared. *Sci. Rep.* **2013**, *3*, 2865.

(11) Aydin, K.; Ferry, V. E.; Briggs, R. M.; Atwater, H. A. Broadband polarization-independent resonant light absorption using ultrathin plasmonic super absorbers. *Nat. Commun.* **2011**, *2*, 517.

(12) Rogers, P. H.; Sirinakis, G.; Carpenter, M. A. Direct observations of electrochemical reactions within Au-YSZ thin films via absorption shifts in the Au nanoparticle surface plasmon resonance. *J. Phys. Chem. C* **2008**, *112*, 6749−6757.

(13) Bagheri, S.; Zgrabik, C. M.; Gissibl, T.; Tittl, A.; Sterl, F.; Walter, R.; De Zuani, S.; Berrier, A.; Stauden, T.; Richter, G.; Hu, E. L.; Giessen, H. Large-area fabrication of TiN nanoantenna arrays for refractory plasmonics in the mid-infrared by Femtosecond direct Laser writing and interference lithography. *Opt. Mater. Express* **2015**, *5*, 2625−2633.

(14) Aksu, S.; Yanik, A. A.; Adato, R.; Artar, A.; Huang, M.; Altug, H. High-throughput nanofabrication of infrared plasmonic nanoantenna arrays for vibrational nanospectroscopy. *Nano Lett.* **2010**, *10*, 2511−2518.

(15) Huebert, T.; Boon-Brett, L.; Black, G.; Banach, U. Hydrogen sensors- a review. *Sens. Actuators, B* **2011**, *157*, 329−352.

(16) Strohfeldt, N.; Tittl, A.; Giessen, H. Long-term stability of capped and buffered palladium-nickel thin films and nanostructures for plasmonic hydrogen sensing applications. *Opt. Mater. Express* **2013**, *3*, 194−204.

(17) Strohfeldt, N.; Tittl, A.; Schaferling, M.; Neubrech, F.; Kreibig, U.; Griessen, R.; Giessen, H. Yttrium hydride nanoantennas for active plasmonics. *Nano Lett.* **2014**, *14*, 1140−1147.

(18) Sterl, F.; Strohfeldt, N.; Walter, R.; Griessen, R.; Tittl, A.; Giessen, H. Magnesium as novel material for active plasmonics in the visible wavelength range. *Nano Lett.* **2015**, *15*, 7949−7955.

(19) Liu, N.; Mesch, M.; Weiss, T.; Hentschel, M.; Giessen, H. Infrared perfect absorber and its application as plasmonic sensor. *Nano Lett.* **2010**, *10*, 2342−2348.

(20) Tittl, A.; Mai, P.; Taubert, R.; Dregely, D.; Liu, N.; Giessen, H. Palladium-based plasmonic perfect absorber in the Visible wavelength range and its application to hydrogen sensing. *Nano Lett.* **2011**, *11*, 4366−4369.

(21) Liu, Z.; Zhan, P.; Chen, J.; Tang, C.; Yan, Z.; Chen, Z.; Wang, Z. Dual broadband near-infrared perfect absorber based on a hybrid plasmonic-photonic microstructure. *Opt. Express* **2013**, *21*, 3021−3030.

(22) Moreau, A.; Ciracì, C.; Mock, J. J.; Hill, R. T.; Wang, Q.; Wiley, B. J.; Chilkoti, A.; Smith, D. R. Controlled-reflectance surfaces with film-coupled colloidal. nanoantennas. *Nature* **2012**, *492*, 86−89.

(23) Zhang, Y.; Wei, T.; Dong, W.; Zhang, K.; Sun, Y.; Chen, X.; Dai, N. Vapor-deposited amorphous metamaterials as visible near-perfect absorbers with random non-prefabricated metal nanoparticles. *Sci. Rep.* **2014**, *4*, 4850.

(24) Wang, D.; Zhu, W.; Best, M. D.; Camden, J. P.; Crozier, K. B. Wafer-scale metasurface for total power absorption, local field enhancement and single molecule Raman spectroscopy. *Sci. Rep.* **2013**, *3*, 2867.

(25) Walter, R.; Tittl, A.; Berrier, A.; Sterl, F.; Weiss, T.; Giessen, H. Large-area low-cost tunable plasmonic perfect absorber in the near infrared by colloidal etching lithography. *Adv. Opt. Mater.* **2015**, *3*, 398−403.

(26) Cattoni, A.; Ghenuche, P.; Haghiri-Gosnet, A.-M.; Decanini, D.; Chen, J.; Pelouard, J.-L.; Collin, S. λ^3/1000 plasmonic nanocavities for biosensing fabricated by soft UV nanoimprint lithography. *Nano Lett.* **2011**, *11*, 3557−3563.

(27) Zhu, J.; Bai, Y.; Zhang, L.; Song, Z.; Liu, H.; Zhou, J.; Lin, T.; Liu, Q. H. Large-scale uniform silver nanocave array for visible light refractive index sensing using soft UV nanoimprint. *IEEE Photonics J.* **2016**, *8*, 6804107.

(28) Bagheri, S.; Giessen, H.; Neubrech, F. Large-area antenna-assisted SEIRA substrates by laser interference lithography. *Adv. Opt. Mater.* **2014**, *2*, 1050−1056.

(29) Xie, Q.; Hong, M. H.; Tan, H. L.; Chen, G. X.; Shi, L. P.; Chong, T. C. Fabrication of nanostructures with laser interference lithography. *J. Alloys Compd.* **2008**, *449*, 261−264.

(30) Asadi, R.; Bagheri, S.; Khaje, M.; Malekmohammad, M.; Tavassoly, M. T. Tunable Fano resonance in large scale polymer-dielectric slab photonic crystals. *Microelectron. Eng.* **2012**, *97*, 201−203.

(31) Meisenheimer, S.-K.; Jüchter, S.; Höhn, O.; Hauser, H.; Wellens, C.; Kübler, V.; von Hauff, E.; Bläsi, B. Large area plasmonic nanoparticle arrays with well-defined size and shape. *Opt. Mater. Express* **2014**, *4*, 944.

(32) Bagheri, S.; Weber, K.; Gissibl, T.; Weiss, T.; Neubrech, F.; Giessen, H. Fabrication of square-centimeter plasmonic nanoantenna arrays by femtosecond direct laser writing lithography: effects of collective excitations on SEIRA enhancement. *ACS Photonics* **2015**, *2*, 779−786.

(33) Malekmohammad, M.; Soltanolkotabi, M.; Erfanian, A.; Asadi, R.; Bagheri, S.; Zahedinejad, M.; Khaje, M.; Naderi, M. H. Broadband photonic crystal antireflection. *JEOS:RP* **2012**, *7*, 12008.

(34) Khanuja, M.; Mehta, B. R.; Agar, P.; Kulriya, P. K.; Avasthi, D. K. Hydrogen induced lattice expansion and crystallinity degradation in palladium nanoparticles: Effect of hydrogen concentration, pressure, and temperature. *J. Appl. Phys.* **2009**, *106*, 093515.

(35) Weiss, T.; Granet, G.; Gippius, N. A.; Tikhodeev, S.; Giessen, H. Matched coordinates and adaptive spatial resolution in the Fourier modal method. *Opt. Express* **2009**, *17*, 8051−8061.

(36) Tittl, A.; Harats, M. G.; Walter, R.; Yin, X.; Schäferling, M.; Liu, N.; Rapaport, R.; Giessen, H. Quantitative angle-resolved small-Spot reflectance measurements on plasmonic perfect absorbers: impedance matching and disorder effects. *ACS Nano* **2014**, *8*, 10885.

(37) Dahlin, A. B.; Tegenfeldt, J. O.; Hook, F. Improving the instrumental resolution of sensors based on localized surface plasmon resonance. *Anal. Chem.* **2006**, *78*, 4416−4423.

(38) Griessen, R.; Strohfeldt, N.; Giessen, H. Thermodynamics of the hybrid interaction of hydrogen with palladium nanoparticles. *Nat. Mater.* **2015**, *15*, 311−317.

(39) Baldi, A.; Narayan, T. C.; Koh, A. L.; Dionne, J. A. In Situ detection of hydrogen-induced phase transitions in individual palladium nanocrystals. *Nat. Mater.* **2014**, *13*, 1143−1148.

(40) Bardhan, R.; Hedges, L. O.; Pint, C. L.; Javey, A.; Whitelam, S.; Urban, J. J. Uncovering the intrinsic size dependence of hydriding phase transformations in nanocrystals. *Nat. Mater.* **2013**, *12*, 905−912.

(41) Fukai, Y. *The metal-hydrogen system: basic bulk properties*; Springer Series in Materials Science; Springer, 2005.

(42) Flanagan, T. B.; Oates, W. A. The palladium-hydrogen system. *Annu. Rev. Mater. Sci.* **1991**, *21*, 269−304.

(43) Suematsu, K.; Sasaki, M.; Ma, N.; Yuasa, M.; Shimanoe, K. Antimony-doped Tin Dioxide gas sensors exhibiting high stability in the sensitivity to humidity changes. *ACS Sensors* **2016**, *1* (7), 913−920.

(44) Strohfeldt, N.; Zhao, J.; Tittl, A.; Giessen, H. Sensitivity engineering in direct contact palladium-gold nano-sandwich hydrogen sensors. *Opt. Mater. Express* **2015**, *5* (11), 2525−2535.

(45) Menumerov, E.; Marks, B. A.; Dikin, D. A.; Lee, F. X.; Winslow, R. D.; Guru, S.; Sil, D.; Borguet, E.; Hutapea, P.; Hughes, R. A.; Neretina, S. Sensing hydrogen gas from atmospheric pressure to a hundred parts per million with nanogaps fabricated using a single-step bending deformation. *ACS Sensors* **2016**, *1* (1), 73−80.